Optica Applicata, Vol. LIII, No. 1, 2023
DOI: 10.37190/oa230106

Manipulating far-field ring-shaped array according to the superposition of weight functions

Chenyuan Yuan, Caifu Yuan, Sufen Xiang, Xiaoling Ji, Tao Wang*

Department of Physics, Sichuan Normal University,
Chengdu 610068, China

*Corresponding author: towerwang@126.com

In order to control the distribution characteristics of the far-field ring-shaped array, we introduce a new light source to produce adjustable far-field distribution by the method of weight function superposition. It has been shown that, by changing the parameters of the light source, one can obtain far-field with various distribution, including distribution with decrease in spectral intensity of specified rings, distribution with disappearances of specified rings, distribution with different spectral intensity of part of lobes in the continuous rings, distribution with part of the lobes in specified rings disappearing and distribution with some lobes in specified rings being stronger. These results will produce some novel far-field distributions which may provide a new idea for further study concerning about the manipulations of far-field array distribution.

Keywords: partially coherent source, optical manipulation, ring-shaped array, spectral density.

1. Introduction

It is an important problem to obtain partially coherent sources which have different characteristics on propagation [1–14]. According to the optical coherence theory, Schell-model source is the most basic and common light source, which is characterized by the spectral degree of coherence between any two points being determined by the difference only. As we all know, the far-field intensity distribution can be changed by changing the structure of the correlation function [15]. In recent years, partially coherent beams with different Gaussian correlated Shell-model functions, which can produce the distribution with different characteristics in the far field were studied [16–23]. For instance, Mei *et al.* discussed a novel source which can produce a ring-shaped far-field array distribution [24] and Zheng *et al.* presented twisted ring-shaped Gaussian Schell -model array source, which can make each lobe in the ring-shaped array rotate clockwise along the propagation distance [25]. These works lay a theoretical basis for the creation of the new sources.

On the other hand, the ring-shaped optical lattice has attracted a lot of interest because of its potential applications, such as quantum field, manipulating for cold atoms or particles and Bose–Einstein condensate [26–31]. Recently, ring-shaped optical lattice has also been applied in other fields such as scattering. For example, WANG and his collaborators controlled distribution of particulate collection, producing a ring-shaped optical lattice distribution [32]. In this study, we will consider the superposition of the weight functions to get a new source and do some novel manipulations in the ring -shaped far-field array distribution. We will first describe the possibility of producing and manipulating a ring-shaped adjustable far-field array produced by ring-shaped adjustable Gaussian Schell model array (RAGSMA) source. Then, the method of how to manipulate the far-field distribution by choosing the parameters of the source has been described in detail.

2. Theory

The properties of light source at a pair of points $\boldsymbol{\rho}_1' = (x_1', y_1')$ and $\boldsymbol{\rho}_2' = (x_2', y_2')$ can be described by the cross-spectral density (CSD) functions $W(\boldsymbol{\rho}_1', \boldsymbol{\rho}_2')$. When the source is the classical Schell-model source, its CSD function can be expressed as [33]

$$W^{(0)}(\boldsymbol{\rho}_1', \boldsymbol{\rho}_2') = \sqrt{S^{(0)}(\boldsymbol{\rho}_1')}\,\sqrt{S^{(0)}(\boldsymbol{\rho}_2')}\,\mu^{(0)}(\boldsymbol{\rho}_2' - \boldsymbol{\rho}_1') \tag{1}$$

where $S^{(0)}(\boldsymbol{\rho}_1')$ and $\mu^{(0)}(\boldsymbol{\rho}_2' - \boldsymbol{\rho}_1')$ are the spectral density and the spectral degree of coherence in the source plane, respectively. To make sure that the source is physically genuine, the sufficient condition should be expressed by the integral [34]

$$W^{(0)}(\boldsymbol{\rho}_1', \boldsymbol{\rho}_2') = \int p(\mathbf{v})\, H_0^*(\boldsymbol{\rho}_1', \mathbf{v})\, H_0(\boldsymbol{\rho}_2', \mathbf{v})\, \mathrm{d}^2 v \tag{2}$$

where $p(\mathbf{v})$ is an arbitrary non-negative weight function, $H_0(\boldsymbol{\rho}', \mathbf{v})$ is an arbitrary kernel and the asterisk stands for complex conjugate. $H_0(\boldsymbol{\rho}', \mathbf{v})$ can be given as a Fourier-like structure for the Schell-model sources [34]

$$H_0(\boldsymbol{\rho}', \mathbf{v}) = \tau(\boldsymbol{\rho}_2') \exp(-2\pi i \mathbf{v} \cdot \boldsymbol{\rho}') \tag{3}$$

where $\tau(\boldsymbol{\rho}')$ is a complex amplitude profile. By substituting Eq. (3) into Eq. (2), one can obtain,

$$W^{(0)}(\boldsymbol{\rho}_1', \boldsymbol{\rho}_2') = \tau^*(\boldsymbol{\rho}_1')\, \tau(\boldsymbol{\rho}_2')\, \mu^{(0)}(\boldsymbol{\rho}_2' - \boldsymbol{\rho}_1') \tag{4}$$

where

$$\mu^{(0)}(\boldsymbol{\rho}_2' - \boldsymbol{\rho}_1') = \int p(\mathbf{v}) \exp\left[-2\pi i \mathbf{v} \cdot (\boldsymbol{\rho}_2' - \boldsymbol{\rho}_1')\right] \mathrm{d}^2 v \tag{5}$$

is the Fourier transform of the weight function $p(\mathbf{v})$. In order to generate a Gaussian array profile in the far-field, we propose the expression for function $p_l(\mathbf{v})$ as [24]

$$p_l(\mathbf{v}) = \frac{2\pi\delta^2}{B}\sum_{n=1}^{N_l}\sum_{j=1}^{nM_l}\exp\left[-2\pi^2(\delta^2 v_x^2+\delta^2 v_y^2)\right]\exp(-2\pi n^2R^2)$$
$$\times\cosh\left[nR(2\pi)^{3/2}\delta(v_x\cos\alpha_j - v_y\sin\alpha_j)\right]$$
$$\times\cosh\left[nR(2\pi)^{3/2}\delta(v_x\sin\alpha_j + v_y\cos\alpha_j)\right] \tag{6}$$

where $l=1, 2, 3, ...$, and $B=N_l(N_l+1)M_l/2$ is the normalization constant, R is arbitrary real constant, δ is the effective correlation length, N_l and M_l are the positive integers used to control the number of the rings and the number of the lobes, respectively, $\cosh(x)$ is the hyperbolic cosine function, and

$$\alpha_j = \frac{\pi j}{2nM} \tag{7}$$

In order to obtain far-field distribution that can be adjusted more flexibly, we propose a new method, *i.e.*, the superposition of the weight functions. In this case, the weight function $p(\mathbf{v})$ can be expressed as follows

$$p(\mathbf{v}) = \sum_{l=1}^{L} a_l p_l(\mathbf{v}) \tag{8}$$

To realize far-field intensity with adjustable arrays distribution, we select three parts for weighted superposition. In this case, the expression of $p(\mathbf{v})$ can be reduced as

$$p(\mathbf{v}) = a p_1(\mathbf{v}) + b p_2(\mathbf{v}) + c p_3(\mathbf{v}) \tag{9}$$

where a, b and c are the weighting factors which can be used to control the spectral intensity of each array, respectively. In this following discussion, parameters a and c are chosen to be positive and b is chosen to be negative. To satisfy the non-negative condition, the value of a is always no smaller than the value of b, and the value of M_1 and N_1 in the weight part of $p_1(\mathbf{v})$ is no smaller than the value of M_2 and N_2 in the weight part of $p_2(\mathbf{v})$, respectively.

By substituting Eq. (6) into (9), then into (5) and setting the amplitude profile function $\tau(\boldsymbol{\rho}')$ as Gaussian profile [25] *i.e.*,

$$\tau(\boldsymbol{\rho}') = \exp\left(-\frac{|\boldsymbol{\rho}'|^2}{4\sigma_0^2}\right) \tag{10}$$

where σ_0 is the source width. The CSD function of RAGSMA source can be written as follows

$$W^{(0)}(x_1', x_2', y_1', y_2') = a W_1^{(0)}(x_1', x_2', y_1', y_2') + b W_2^{(0)}(x_1', x_2', y_1', y_2') + c W_3^{(0)}(x_1', x_2', y_1', y_2') \tag{11}$$

As an example, we will discuss far-field with adjustable ring-shaped arrays distribution. Therefore, we chose each part in Eq. (11) to be ring-shaped arrays distribution, which can be expressed as [35]

$$W_l^{(0)}(x_1', x_2', y_1', y_2')$$

$$= \frac{1}{B}\exp\left(-\frac{(x_1')^2+(y_1')^2}{4\sigma_0^2}-\frac{(x_2')^2+(y_2')^2}{4\sigma_0^2}\right)\exp\left(-\frac{(x_2'-x_1')^2+(y_2'-y_1')^2}{2\delta^2}\right)$$

$$\times\sum_{n=1}^{N_l}\sum_{j=1}^{nM_l}\cos\left\{\frac{1}{\delta}\sqrt{2\pi}\,nR\left[(x_2'-x_1')\cos\alpha_j-(y_2'-y_1')\sin\alpha_j\right]\right\}$$

$$\times\cos\left\{\frac{1}{\delta}\sqrt{2\pi}\,nR\left[(x_2'-x_1')\sin\alpha_j+(y_2'-y_1')\cos\alpha_j\right]\right\} \tag{12}$$

Now, let us consider the characteristics produced by the RAGSMA source in the half-space $z > 0$. The propagation CSD function in the far-field at two points $\mathbf{r}_1 = r_1\mathbf{s}_1$ and $\mathbf{r}_2 = r_2\mathbf{s}_2$ has the form [33]

$$W^{(\infty)}(\mathbf{r}_1, \mathbf{r}_2) = (2\pi k)^2\cos\theta_1\cos\theta_2\,\tilde{W}^{(0)}(-k\,\mathbf{s}_{1\perp}, k\,\mathbf{s}_{2\perp})\frac{\exp\left[ik(\mathbf{r}_2-\mathbf{r}_1)\right]}{\mathbf{r}_1\mathbf{r}_2} \tag{13}$$

where the notation related to the far-field is presented in Fig. 1, and $k = 2\pi/\lambda$ is the wave number, $\mathbf{s}_1$ and $\mathbf{s}_2$ are unit vectors, θ_1 and θ_2 are angles made by $\mathbf{s}_1$ and $\mathbf{s}_2$ in the positive z-axis, $\mathbf{s}_{1\perp} = \sin\theta_1$, $\mathbf{s}_{2\perp} = \sin\theta_2$, and

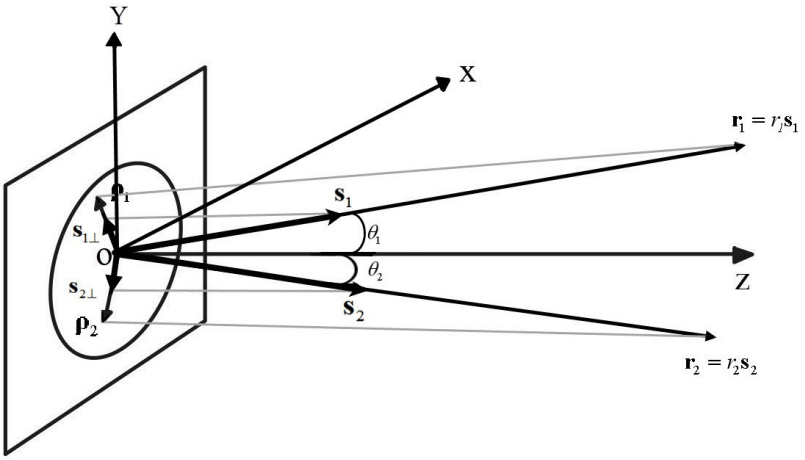

Fig. 1. Illustration of the notation related to the far-field.

$$\tilde{W}^{(0)}(\mathbf{f}_1, \mathbf{f}_2) = \frac{1}{(2\pi)^4} \iint W^{(0)}(\boldsymbol{\rho}_1', \boldsymbol{\rho}_2') \exp\left[-i(\mathbf{f}_1 \cdot \boldsymbol{\rho}_1' + \mathbf{f}_2 \cdot \boldsymbol{\rho}_2')\right] \mathrm{d}^2\boldsymbol{\rho}_1' \, \mathrm{d}^2\boldsymbol{\rho}_2' \tag{14}$$

By substituting Eq. (11) and (12) first into Eq. (14), and then into (13), one can obtain the CSD function of the far-field generated by the RAGSMA source, and it has the following form

$$W^{(\infty)}(x_1', x_2', y_1', y_2')$$

$$= a W_1^{(\infty)}(x_1', x_2', y_1', y_2') + b W_2^{(\infty)}(x_1', x_2', y_1', y_2') + c W_3^{(\infty)}(x_1', x_2', y_1', y_2') \tag{15}$$

where

$$W_l^{(\infty)}(\mathbf{r}_1, \mathbf{r}_2) = \frac{k^2 \sigma_0^2 \cos\theta_1 \cos\theta_2 \exp\left[ik(\mathbf{r}_2 - \mathbf{r}_1)\right]}{8\Theta B \mathbf{r}_1 \mathbf{r}_2}$$

$$\times \sum_{n=1}^{N_l} \sum_{j=1}^{nM_l} \exp\left(-\frac{k^2\sigma_0^2(s_{2x} - s_{1x})^2}{2} - \frac{k^2(s_{2x} + s_{1x})^2}{16\Theta}\right) \exp\left(-\frac{n^2 R^2 \pi}{2\Theta\delta^2}\right)$$

$$\times \exp\left(-\frac{k^2\sigma_0^2(s_{2y} - s_{1y})^2}{2} - \frac{k^2(s_{2y} + s_{1y})^2}{16\Theta}\right) \exp\left(-\frac{n^2 R^2 \pi}{2\Theta\delta^2}\right)$$

$$\times \left\{ \exp\left[\Delta_x(\cos\alpha_j + \sin\alpha_j) + \Delta_y(\cos\alpha_j - \sin\alpha_j)\right] \right.$$

$$+ \exp\left[\Delta_x(\cos\alpha_j - \sin\alpha_j) + \Delta_y(-\cos\alpha_j - \sin\alpha_j)\right]$$

$$+ \exp\left[\Delta_x(-\cos\alpha_j + \sin\alpha_j) + \Delta_y(\cos\alpha_j + \sin\alpha_j)\right]$$

$$\left. + \exp\left[\Delta_x(-\cos\alpha_j - \sin\alpha_j) + \Delta_y(-\cos\alpha_j + \sin\alpha_j)\right] \right\} \tag{16}$$

where s_{1x}, s_{1y} are the projection of $\mathbf{s}_1$ onto the x- and y-axes, respectively, and s_{2x}, s_{2y} are the projection of $\mathbf{s}_2$ onto the x- and y-axes, respectively, and

$$\Theta = \frac{1}{8\sigma_0^2} + \frac{1}{2\delta^2} \tag{17a}$$

$$\Delta_x = \frac{nRk\sqrt{2\pi}}{4a\delta}(s_{2x} + s_{1x}) \tag{17b}$$

$$\Delta_y = \frac{nRk\sqrt{2\pi}}{4a\delta}(s_{2y} + s_{1y}) \tag{17c}$$

Then, the spectral density can be calculated by letting the two points to coincide, *i.e.*, $\mathbf{r}_1 = \mathbf{r}_2 = \mathbf{r}$. After a simple calculation, one can express the spectral density as follows

$$S^{(\infty)}(\mathbf{r}) = aS_1^{(\infty)}(\mathbf{r}) + bS_2^{(\infty)}(\mathbf{r}) + cS_3^{(\infty)}(\mathbf{r}) \tag{18}$$

where

$$\begin{aligned} S_l^{(\infty)}(\mathbf{r}) = {} & \frac{k^2\sigma_0^2\cos^2\theta}{8\Theta Br^2} \\ & \times \sum_{n=1}^{N_l}\sum_{j=1}^{nM_l} \exp\left(-\frac{k^2 s_x^2}{4\Theta} - \frac{n^2R^2\pi}{2\Theta\delta^2}\right)\exp\left(-\frac{k^2 s_y^2}{4\Theta} - \frac{n^2R^2\pi}{2\Theta\delta^2}\right) \\ & \times \Big\{ \exp\left[\Delta_x'(\cos\alpha_j + \sin\alpha_j) + \Delta_y'(\cos\alpha_j - \sin\alpha_j)\right] \\ & + \exp\left[\Delta_x'(\cos\alpha_j - \sin\alpha_j) + \Delta_y'(-\cos\alpha_j - \sin\alpha_j)\right] \\ & + \exp\left[\Delta_x'(-\cos\alpha_j + \sin\alpha_j) + \Delta_y'(\cos\alpha_j + \sin\alpha_j)\right] \\ & + \exp\left[\Delta_x'(-\cos\alpha_j - \sin\alpha_j) + \Delta_y'(-\cos\alpha_j + \sin\alpha_j)\right] \Big\} \end{aligned} \tag{19}$$

and

$$\Delta_x' = \frac{nRk\sqrt{2\pi}}{2\Theta\delta}s_x, \qquad \Delta_y' = \frac{nRk\sqrt{2\pi}}{2\Theta\delta}s_y \tag{20}$$

3. Numerical simulations

In above sections, the RAGSMA source which can produce and manipulate its ring -shaped adjustable far-field array has been discussed. Now, let us analyze the distribution of the ring-shaped array in the far-field which is controlled by properly changing the parameters of the RAGSMA source. The details are as follows: Figure 2 shows that the spectral intensity of specified rings can be decreased by selecting different values of a, b, c, and N_l. The spectral intensity shows ring-shaped array distribution with specified rings decreased, *i.e.*, a ring-shaped array distribution with weaker spectral intensity in the first ring (see Fig. 2(a)), a ring-shaped array distribution with weaker spectral intensity in the second ring (see Fig. 2(b)) and a ring-shaped array distribution with weaker spectral intensity in the first and second rings (see Fig. 2(c)). In other words, we can decrease the spectral intensity of the ring by properly changing the parameters a, b, c, and N_l.

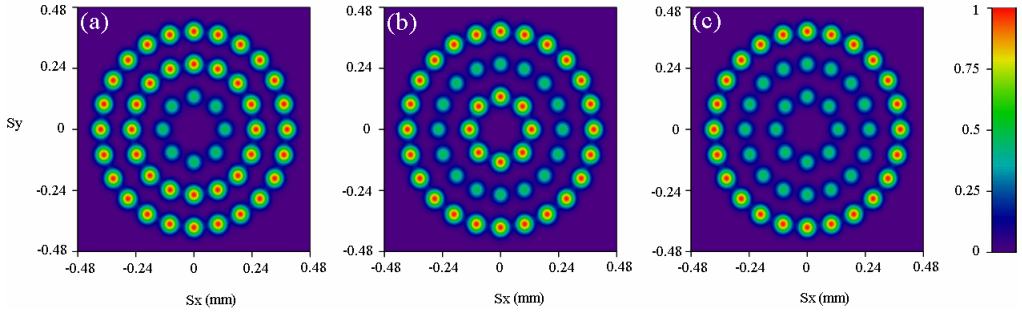

Fig. 2. Control of spectral intensity of the specified rings in the array. Calculated parameters are set as follows: $R = 1.8$, $\delta = 0.5$ mm, $\sigma_0 = 0.5$ mm, and $\lambda = 632 \times 10^{-9}$ m. (a) $a = 1$, $N_1 = 3$, $M_1 = 2$, $b = -0.5$, $N_2 = 1$, $M_2 = 2$; (b) $a = 1$, $N_1 = 3$, $M_1 = 2$, $b = -0.5$, $N_2 = 2$, $M_2 = 2$, $c = 0.5$, $N_3 = 1$, $M_3 = 2$; (c) $a = 1$, $N_1 = 3$, $M_1 = 2$, $b = -0.5$, $N_2 = 2$, $M_2 = 2$.

Figure 3 shows the control of the disappearance of specified rings. Here, in order to make the ring disappear, we have set the parameters $M_1 = M_2 = M_3 = 2$. As shown in Fig. 3, by selecting different values of a, b, c, and N_l the spectral intensity shows ring-shaped array distribution with specified rings disappeared, *i.e.*, a ring-shaped array distribution with the first ring disappeared (see Fig. 3(a)), a ring-shaped array distribution with the second ring disappeared (see Fig. 3(b)), and a ring-shaped array distribution with the first and second rings disappeared (see Fig. 3(c)). Therefore, we can manipulate the disappearance of the ring by properly changing the parameters a, b, c, and N_l of the source.

Figure 4 shows how to manipulate the spectral intensity of part of lobes in the continuous rings. Here, in order to make the continuous rings, we have set the parameter $M_1 = 8$. As shown in Fig. 4, by selecting different values of a, b, c, N_l and M_2, the spec-

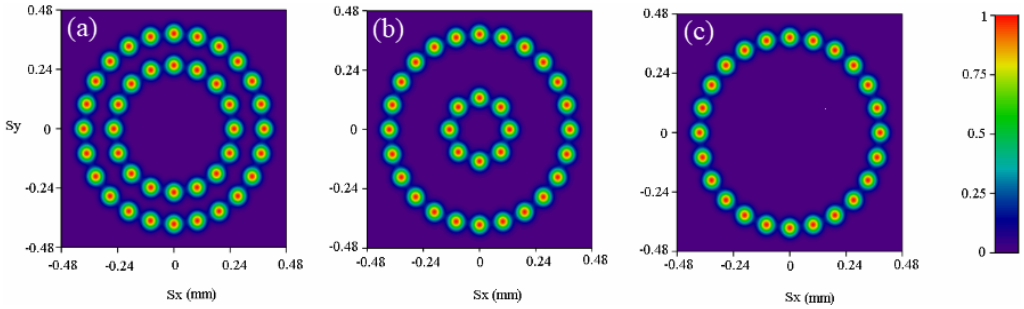

Fig. 3. Control of appearance of the specified rings in the array. Calculated parameters are set as follows: $R = 1.8$, $\delta = 0.5$ mm, $\sigma_0 = 0.5$ mm, and $\lambda = 632 \times 10^{-9}$ m. (a) $a = 1$, $N_1 = 3$, $M_1 = 2$, $b = -1$, $N_2 = 1$, $M_2 = 2$; (b) $a = 1$, $N_1 = 3$, $M_1 = 2$, $b = -1$, $N_2 = 2$, $M_2 = 2$, $c = 1$, $N_3 = 1$, $M_3 = 2$; (c) $a = 1$, $N_1 = 3$, $M_1 = 2$, $b = -1$, $N_2 = 2$, $M_2 = 2$.

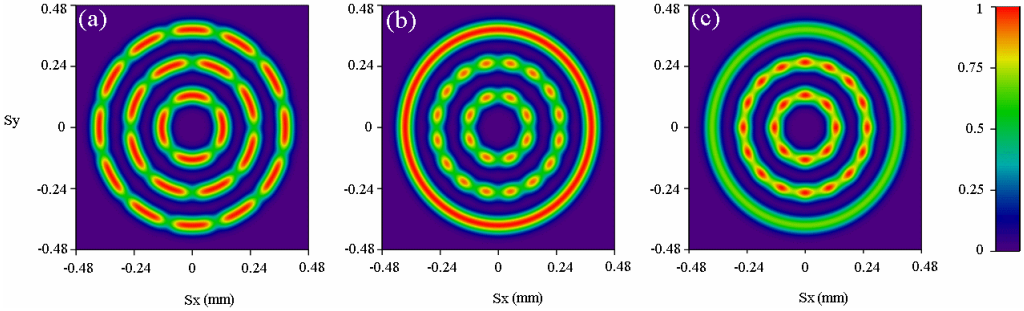

Fig. 4. Change the spectral intensity of part of lobes in the continuous rings. Calculated parameters are set as follows: $R = 1.8$, $\delta = 0.5$ mm, $\sigma_0 = 0.5$ mm, and $\lambda = 632 \times 10^{-9}$ m. (a) $a = 1$, $N_1 = 3$, $M_1 = 8$, $b = -1$, $N_2 = 3$, $M_2 = 1$; (b) $a = 1$, $N_1 = 3$, $M_1 = 8$, $b = -1$, $N_2 = 2$, $M_2 = 2$; (c) $a = 1$, $N_1 = 3$, $M_1 = 8$, $b = 1$, $N_2 = 2$, $M_2 = 2$.

tral intensity shows ring-shaped array distribution with different spectral intensity of part of lobes in the continuous rings, *i.e.*, a ring-shaped array distribution with the spectral intensity of part of lobes in each continuous ring being weaker than the others (see Fig. 4(a)), a ring-shaped array distribution with the spectral intensity of part of lobes in the first and second continuous rings being weaker than the others with a stronger third ring (see Fig. 4(b)) and a ring-shaped array distribution with the spectral intensity of part of lobes in the first and second continuous rings being stronger than the others with a weaker third ring (see Fig. 4(c)). Thus, we can manipulate the spectral intensity of part of lobes in the continuous rings by changing the parameters a, b, c, N_l and M_l of the source.

Figure 5 shows that we can control the disappearance of part of the lobes in the specified rings. Here, in order to make part of the lobes in the specified rings disappear, we have set the parameters $M_1 = 2$ and $M_2 = M_3 = 1$. As shown in Fig. 5, by selecting different values of a, b, c, and N_l, the spectral intensity shows ring-shaped array dis-

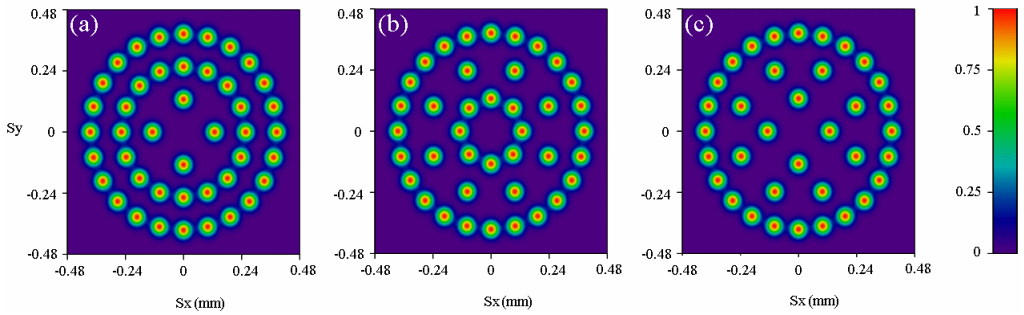

Fig. 5. Control of part of the lobes on the specified rings in the array. Calculated parameters are set as follows: $R = 1.8$, $\delta = 0.5$ mm, $\sigma_0 = 0.5$ mm, and $\lambda = 632 \times 10^{-9}$ m. (a) $a = 1$, $N_1 = 3$, $M_1 = 2$, $b = -1$, $N_2 = 1$, $M_2 = 1$; (b) $a = 1$, $N_1 = 3$, $M_1 = 2$, $b = -1$, $N_2 = 2$, $M_2 = 1$, $c = 1$, $N_3 = 1$, $M_3 = 1$; (c) $a = 1$, $N_1 = 3$, $M_1 = 2$, $b = -1$, $N_2 = 2$, $M_2 = 1$.

tribution with part of the lobes in the specified rings disappeared, *i.e.*, a ring-shaped array distribution with part of the lobes of the first ring disappeared (see Fig. 5(a)), a ring-shaped array distribution with part of the lobes of the second ring disappeared (see Fig. 5(b)) and a ring-shaped array distribution with part of the lobes of the first and second rings disappeared (see Fig. 5(c)). Thus, we can make some lobes of the ring disappear by properly changing the parameters a, b, c, and N_l.

Figure 6 shows that we can make some lobes on a particular ring stronger. Here, in order to avoid the overlap of the lobes, we have set the parameters $M_1 = 2$, $M_2 = 1$ and $M_3 = 2$. As shown in Fig. 6, by selecting different values of a, b, c, and N_l, the spectral intensity shows ring-shaped array distribution with some lobes on a particular ring being stronger, *i.e.*, a ring-shaped array distribution with the spectral intensity of part of the lobes in the first ring being stronger than others (see Fig. 6(a)), a ring-shaped array distribution that the spectral intensity of part of the lobes in the first and second rings being stronger than others (see Fig. 6(b)) and a ring-shaped array distribution with

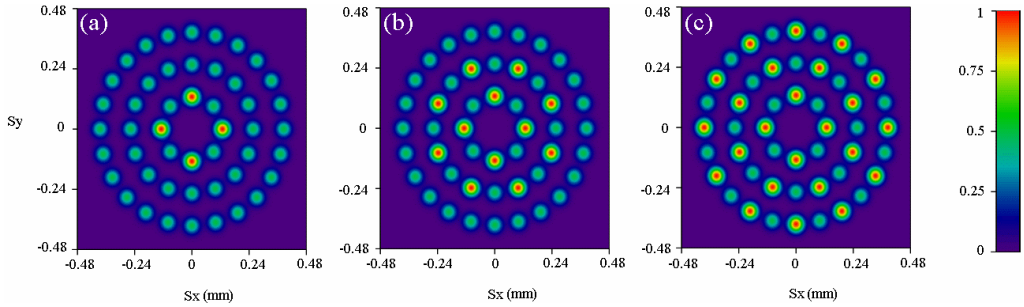

Fig. 6. Control of spectral intensity of several lobes of the specified rings in the array. Calculated parameters are set as follows: $R = 1.8$, $\delta = 0.5$ mm, $\sigma_0 = 0.5$ mm, and $\lambda = 632 \times 10^{-9}$ m. (a) $a = 1$, $N_1 = 3$, $M_1 = 2$, $b = -1$, $N_2 = 1$, $M_2 = 1$, $c = 1$, $N_3 = 1$, $M_3 = 2$; (b) $a = 1$, $N_1 = 3$, $M_1 = 2$, $b = -1$, $N_2 = 2$, $M_2 = 1$, $c = 1$, $N_3 = 2$, $M_3 = 2$; (c) $a = 1$, $N_1 = 3$, $M_1 = 2$, $b = -1$, $N_2 = 3$, $M_2 = 1$, $c = 1$, $N_3 = 3$, $M_3 = 2$.

the spectral intensity of part of the lobes in each rings being stronger than others (see Fig. 6(c)). Therefore, part of the lobes in the specified rings can be stronger by manipulating the parameters a, b, c, and N_l.

4. Conclusions

In conclusion, we have discussed a new source which can generate adjustable distributions in the far-field. We analyzed the adjustable distribution in the far-field by changing the parameters. It has been shown that the characteristics of far-zone field spectral intensity, including the decrease of spectral intensity of specified rings, the disappearance of specified rings, the difference of spectral intensity of part of lobes in the continuous rings, the disappearance of part of the lobes in specified rings and the decrease of spectral intensity of some lobes in specified rings, can be manipulated by adjusting the corresponding parameters of the source. Specifically, the number of rings can be manipulated by the parameter N, the number of lobes in each ring can be manipulated by the parameter M, and the intensity of each ring can be adjusted by properly choosing parameters a, b and c.

Acknowledgement
This work was supported by the National Natural Science Foundation of China (NSFC) under grants 11404231, 61475105.

References

[1] WOLF E., COLLETT E., *Partially coherent sources which produce the same far-field intensity distribution as a laser*, Optics Communications **25**(3), 1978: 293–296, DOI: 10.1016/0030-4018(78)90131-1.
[2] MARTÍNEZ-HERRERO R., MEJÍAS P.M., *Radiometric definitions for partially coherent sources*, Journal of the Optical Society of America A **1**(5), 1984: 556–558, DOI: 10.1364/JOSAA.1.000556.
[3] GORI F., GUATTARI G., PADOVANI C., *Modal expansion for J_0-correlated Schell-model sources*, Optics Communications **64**(4), 1987: 311–316, DOI: 10.1016/0030-4018(87)90242-2.
[4] SIMON R., MUKUNDA N., *Twisted Gaussian Schell-model beams*, Journal of the Optical Society of America A **10**(1), 1993: 95–109, DOI: 10.1364/JOSAA.10.000095.
[5] GORI F., BAGINI V., SANTARSIERO M., FREZZA F., SCHETTINI G., SPAGNOLO G.S., *Coherent and partially coherent twisting beams*, Optical Review **1**(2), 1994: 143–145, DOI: 10.1007/BF03254845.
[6] PONOMARENKO S.A., *A class of partially coherent beams carrying optical vortices*, Journal of the Optical Society of America A **18**(1), 2001: 150–156, DOI: 10.1364/JOSAA.18.000150.
[7] SHCHEGROV A.V., WOLF E., *Partially coherent conical beams*, Optics Letters **25**(3), 2000: 141–143, DOI: 10.1364/OL.25.000141.
[8] BOGATYRYOVA G.V., FEL'DE C.V., POLYANSKII P.V., PONOMARENKO S.A., SOSKIN M.S., WOLF E., *Partially coherent vortex beams with a separable phase*, Optics Letters **28**(11), 2003: 878–880, DOI: 10.1364/OL.28.000878.
[9] KOROTKOVA O., ANDREWS L.C., PHILLIPS R.L., *Model for a partially coherent Gaussian beam in atmospheric turbulence with application in Lasercom*, Optical Engineering **43**(2), 2004: 330–341, DOI: 10.1117/1.1636185.
[10] VAHIMAA P., TURUNEN J., *Finite-elementary-source model for partially coherent radiation*, Optics Express **14**(4), 2006: 1376–1381, DOI: 10.1364/OE.14.001376.

[11] GORI F., SANTARSIERO M., BORGHI R., LI C.F., *Partially correlated thin annular sources: the scalar case*, Journal of the Optical Society of America A **25**(11), 2008: 2826–2832, DOI: 10.1364/JOSAA.25.002826.

[12] MARTÍNEZ-HERRERO R., MEJÍAS P.M., GORI F., *Genuine cross-spectral densities and pseudo-modal expansions*, Optics Letters **34**(9), 2009: 1399–1401, DOI: 10.1364/OL.34.001399.

[13] LAJUNEN H., SAASTAMOINEN T., *Propagation characteristics of partially coherent beams with spatially varying correlations*, Optics Letters **36**(20), 2011: 4104–4106, DOI: 10.1364/OL.36.004104.

[14] KOROTKOVA O., SAHIN S., SHCHEPAKINA E., *Multi-Gaussian Schell-model beams*, Journal of the Optical Society of America A **29**(10), 2012: 2159–2164, DOI: 10.1364/JOSAA.29.002159.

[15] MANDEL L., WOLF E., SHAPIRO J.H., *Optical coherence and quantum optics*, Physics Today **49**(5) 1996: 68–70, DOI: 10.1063/1.2807623.

[16] CAI Y., WANG F., *Tensor method for treating the propagation of scalar and electromagnetic Gaussian Schell-model beams: A review*, The Open Optics Journal **4**(5), 2010: 1–20, DOI: 10.2174/1874328501004010001.

[17] CAI Y., *Generation of various partially coherent beams and their propagation properties in turbulent atmosphere: A review*, Proc. SPIE **7924**, Atmospheric and Oceanic Propagation of Electromagnetic Waves V, 2011: 792402, DOI: 10.1117/12.878821.

[18] CAI Y., WANG F., ZHAO C., ZHU S., WU G., DONG Y., *Partially coherent vector beams: from theory to experiment*, [In] *Vectorial Optical Fields:Fundamentals and Applications*, Chap. 7: 221–273.

[19] LIU X., WANG F., WEI C., CAI Y., *Experimental study of turbulence-induced beam wander and deformation of a partially coherent beam*, Optics Letters **39**(11), 2014: 3336–3339, DOI: 10.1364/OL.39.003336.

[20] LIU X., SHEN Y., LIU L., WANG F., CAI Y., *Experimental demonstration of vortex phase-induced reduction in scintillation of a partially coherent beam*, Optics Letters **38**(24), 2013: 5323–5326, DOI: 10.1364/OL.38.005323.

[21] WANG F., LIU X., LIU L., YUAN Y., CAI Y., *Experimental study of the scintillation index of a radially polarized beam with controllable spatial coherence*, Applied Physics Letters **103**(9), 2013: 091102, DOI: 10.1063/1.4819202.

[22] DONG Y., WANG F., ZHAO C., CAI Y., *Effect of spatial coherence on propagation, tight focusing and radiation forces of an azimuthally polarized beam*, Physical Review A **86**(1), 2012: 013840, DOI: 10.1103/PhysRevA.86.013840.

[23] ZHAO C., WANG F., DONG Y., HAN Y., CAI Y., *Effect of spatial coherence on determining the topological charge of a vortex beam*, Applied Physics Letters **101**(26), 2012: 261104, DOI: 10.1063/1.4773236.

[24] MEI Z., KOROTKOVA O., *Random sources generating ring-shaped beams*, Optics Letters **38**(2), 2013: 91–93, DOI: 10.1364/OL.38.000091.

[25] ZHENG S., YUAN C., CHENG K., JI X., WANG T., *Ring-shaped hollow multi-Gaussian Schell-model array beams*, Optik **218**, 2020: 165025, DOI: 10.1016/j.ijleo.2020.165025.

[26] MACDONALD M.P., PATERSON L., VOLKE-SEPULVEDA K., ARLT J., SIBBETT W., DHOLAKIA K., *Creation and manipulation of three-dimensional optically trapped structures*, Science, **296**(5570), 2002: 1101–1103, DOI: 10.1126/science.1069571.

[27] FRANKE-ARNOLD S., LEACH J., PADGETT M.J., LEMBESSIS V.E., ELLINAS D., WRIGHT A.J., GIRKIN J.M., OHBERG P., ARNOLD A.S., *Optical ferris wheel for ultracold atoms*, Optics Express **15**(14), 2007: 8619–8625, DOI: 10.1364/OE.15.008619.

[28] AMICO L., OSTERLOH A., CATALIOTTI F., *Quantum many particle systems in ring-shaped optical lattices*, Physical Review Letters **95**(6), 2005: 063201, DOI: 10.1103/PhysRevLett.95.063201.

[29] JEZEK D.M., CATALDO H.M., *Multimode model for an atomic Bose–Einstein condensate in a ring-shaped optical lattice*, Physical Review A **88**(1), 2013: 013636, DOI: 10.1103/PhysRevA.88.013636.

[30] CATALDO H.M., JEZEK D.M., *Bose-Hubbard model in a ring-shaped optical lattice with high filling factors*, Physical Review A **84**(1), 2011: 013602, DOI: 10.1103/PhysRevA.84.013602.

[31] AMICO L., AGHAMALYAN D., AUKSZTOL F., CREPAZ H., DUMKE R., KWEK L.C., *Superfluid qubit systems with ring shaped optical lattices*, Scientific Reports **4**(1), 2014: 04298, DOI: 10.1038/srep04298.
[32] ZHU Z., WU H., CHENG K., WANG T., *Ring-shaped optical coherence lattice distribution produced by light waves on scattering*, Optics Communications **434**, 2019: 157–162, DOI: 10.1016/j.optcom.2018.10.050.
[33] MANDEL L., WOLF E., *Optical Coherence and Quantum Optics*, Cambridge University Press.
[34] GORI F., SANTARSIERO M., *Devising genuine spatial correlation functions*, Optics Letters **32**(24), 2007: 3531–3533, DOI: 10.1364/OL.32.003531.
[35] MAO Y., MEI Z., *Random sources generating ring-shaped optical lattice*, Optics Communications **381**, 2016: 222–226, DOI: 10.1016/j.optcom.2016.06.091.

Received March 7, 2022
in revised form May 13, 2022